Video Article

Studying Soft-matter and Biological Systems over a Wide Length-scale from Nanometer and Micrometer Sizes at the Small-angle Neutron Diffractometer KWS-2

Aurel Radulescu[1], Noemi Kinga Szekely[1], Marie-Sousai Appavou[1], Vitaliy Pipich[1], Thomas Kohnke[1], Vladimir Ossovyi[1], Simon Staringer[1], Gerald J. Schneider[2], Matthias Amann[3], Bo Zhang-Haagen[3], Georg Brandl[1], Matthias Drochner[4], Ralf Engels[4], Romuald Hanslik[5], Günter Kemmerling[1]

[1]Jülich Centre for Neutron Science Outstation at MLZ, Forschungszentrum Jülich GmbH

[2]Department of Chemistry, Louisiana State University

[3]Jülich Centre for Neutron Science JCNS-1 & Institute of Complex Systems ICS-1, Forschungszentrum Jülich GmbH

[4]Central Institute of Engineering, Electronics and Analytics — Electronic Systems (ZEA-2), Forschungszentrum Jülich GmbH

[5]Central Institute of Engineering, Electronics and Analytics — Engineering and Technology (ZEA-1), Forschungszentrum Jülich GmbH

Correspondence to: Aurel Radulescu at a.radulescu@fz-juelich.de

Abstract

The KWS-2 SANS diffractometer is dedicated to the investigation of soft matter and biophysical systems covering a wide length scale, from nm to μm. The instrument is optimized for the exploration of the wide momentum transfer Q range between 1×10^{-4} and 0.5 Å^{-1} by combining classical pinhole, focusing (with lenses), and time-of-flight (with chopper) methods, while simultaneously providing high-neutron intensities with an adjustable resolution. Because of its ability to adjust the intensity and the resolution within wide limits during the experiment, combined with the possibility to equip specific sample environments and ancillary devices, the KWS-2 shows a high versatility in addressing the broad range of structural and morphological studies in the field. Equilibrium structures can be studied in static measurements, while dynamic and kinetic processes can be investigated over time scales between minutes to tens of milliseconds with time-resolved approaches. Typical systems that are investigated with the KWS-2 cover the range from complex, hierarchical systems that exhibit multiple structural levels (*e.g.,* gels, networks, or macro-aggregates) to small and poorly-scattering systems (*e.g.,* single polymers or proteins in solution). The recent upgrade of the detection system, which enables the detection of count rates in the MHz range, opens new opportunities to study even very small biological morphologies in buffer solution with weak scattering signals close to the buffer scattering level at high Q.

In this paper, we provide a protocol to investigate samples with characteristic size levels spanning a wide length scale and exhibiting ordering in the mesoscale structure using KWS-2. We present in detail how to use the multiple working modes that are offered by the instrument and the level of performance that is achieved.

Video Link

The video component of this article can be found at http://www.jove.com/video/54639/

Introduction

Soft and biological materials show a rich variety of morphologies that are characterized by features such as self-organization and self-assembly of elementary units to larger, complex aggregates. They also show cooperative interplay with a large number of degrees of freedom; weak interaction between the structural units, and thus high sensitivity to external fields; and spatiotemporal correlations that can span a broad range, from nanometers to millimeters and from nanoseconds to days. Because of the large range of relevant length- and timescales, the experimental characterization of the properties of these materials are very challenging. Scattering techniques with neutrons play an important role in the investigation of the structure, dynamics, and thermodynamic properties of such complex systems. As unique probes, neutrons offer the advantage of different interactions between the ^{1}H and [2]H (deuterium, D) hydrogen isotopes. The large difference in the coherent scattering length density between hydrogen and deuterium represents the basis of the contrast variation and contrast matching methods. As most of the soft matter and biological systems consist of hydrocarbons, hydrogen/deuterium (H/D) substitution offers the possibility to vary the coherent scattering length density of a compound over a broad range. With this technique, selected constituents in a complex system can be labeled by isotope exchange. Depending on its contrast-the squared difference between its scattering length density and that of the other components-selected components or regions within a complex soft matter or biophysical morphology can be made visible or invisible in the scattering experiment without chemically altering the system. Furthermore, neutrons are highly penetrating and can be used as non-destructive probes and

for studying samples in special environments, where the contribution from the additional materials placed in the beam can be reliably measured and corrected for.

Elastic scattering experiments deliver information about the structure and morphology of a sample. The scattered intensity is measured in reciprocal space as a function of the momentum transfer Q, where $Q = 4\pi/\lambda \sin\Theta/2$, with λ - the neutron wavelength and Θ - the scattering angle; this is then translated into real space through an inverse Fourier transformation. Thus, large Q values relate to short length scales, with the inter-atomic correlations investigated by classical neutron diffraction (ND). At small Q values, large length scales can be explored by small-angle neutron scattering (SANS). Typically, single or assembling synthetic or natural macromolecules in solution, melt, film, or bulk samples are characterized over a wide length scale, from nanometer and micrometer sizes, via the application of the classical pin-hole SANS and the ultra-SANS (based on focusing or single-crystal diffractometry) techniques. However, the combination of different methods or facilities for achieving a complete structural characterization is sometimes difficult because of issues such as available amount of sample, stability of samples over long timescales, reproducibility of effects in special thermodynamic conditions, and the joint analysis of experimental data obtained in different experimental geometries. Moreover, the studies that deal with structures and fast structural changes that are characterized by high space or time resolution are very challenging, requiring very special experimental setups. Therefore, the development of highly versatile SANS instruments, where limits can be pushed beyond the typical configuration in an easy and practicable manner, is beneficial for meeting all special demands from the user community.

The SANS diffractometer KWS-2 (**Figure 1**), operated by the Jülich Centre of Neutron Science (JCNS) at the Heinz Maier-Leibnitz Center (MLZ) in Garching, was originally a classical pinhole SANS instrument benefiting from a high neutron flux (**Supplementary Figure 1**) delivered by the FRM II neutron source[1] and the dedicated guide system[2-4]. After repeated upgrades, the instrument was optimized for the exploration of a wide Q range, between 1×10^{-4} and 0.5 Å^{-1}, providing high neutron intensities and an adjustable resolution. With the availability of specific sample environments and ancillary devices (**Table 1**), the instrument can be equipped to study soft matter and biophysical systems over a wide length scale, from nm up to μm, through static measurements; it can also perform time-resolved investigations of structures and morphologies at equilibrium or under transformation due to kinetic processes, spanning a wide time scale between minutes and tens of milliseconds. In conventional working mode (**Figure 2A**), a Q range between 7×10^{-4} Å^{-1} and 0.5 Å^{-1} can be covered through the variation of the sample-to-detector distance and/or the wavelength. Therefore, structural levels and correlation effects on a length scale from 10 Å up to 9,000 Å can be inspected in real space (where the dimension is considered as $2\pi/Q$). The selection of the wavelength, between 4.5 Å and 20 Å, using a mechanical monochromator (velocity selector) that provides a wavelength spread $\Delta\lambda/\lambda = 20\%$, the variation of the collimation conditions (collimation length L_C and aperture openings, A_C- the entrance aperture, following the last neutron guide segment in beam, and A_S- the sample aperture, just in front of the sample) and of detection distance L_D are done automatically, via computer control.

Considerable upgrades on the intensity on the sample, the instrument resolution, the minimum momentum transfer Q_m, and the fast detection at high count rates in the MHz range were carried out recently, aiming to boost the instrument performance. During this process, the instrument was equipped with additional features.

There is a double-disc chopper[5] with variable slit openings (**Supplementary Figure 2**) and time-of-flight (TOF) data acquisition mode. The chopper can be operated at a varying frequency $f_{chopper}$ between 10 Hz and 100 Hz and at angular openings of the two chopper windows between angles of $0° \leq \Delta\varphi \leq 90°$ by changing the positioning of the two discs with respect to each other. The improvement in wavelength resolution $\Delta\lambda/\lambda$ is achieved by shortening the opening time of the neutron guide τ_w by decreasing $\Delta\varphi$ and/or increasing $f_{chopper}$. The resulting pulses recorded on the detector are split in an appropriate number of time channels that match τ_w in width and are characterized by the aimed $\Delta\lambda/\lambda$.

There are also focusing elements made of magnesium fluorite MgF_2 parabolic lenses[6] with a diameter of 50 mm (**Figure 1**). 26 MgF_2 lenses are grouped into three packages (4+6+16 lenses) that can be moved independently in the beam to achieve focusing conditions with different wavelengths $\lambda = 7$-20 Å. In order to increase the transmission by reducing the scattering on phonons in the lens material, the lenses are kept at 70 K using a special cooling system.

There is a secondary high-resolution position-sensitive scintillation detector with a 1 mm position resolution and a 0.45 mm pixel-size. The detector is typically placed in the tower on the top of the vacuum tank at a fixed distance $L_D = 17$ m and can be vertically moved in or out of the beam (**Figure 1**). The main detector is parked in the end position of the tank at 20 m, while the secondary detector is moved in the beam when high-resolution investigations (low Q) using lenses are being performed[4,7]. The secondary detector is placed in one focal point of the lens system, while a small entrance aperture at $L_C = 20$ m would be, in this case, in the other focal point.

There is a new main detection system that consists of an array of 144 ^{3}He tubes (with a global efficiency per tube of 85% for $\lambda = 5$ Å) and that defines an active detection area equivalent to 0.9 m^2 (**Figure 1**). Innovative rapid readout electronics mounted in a closed case on the backside of the ^{3}He tube frame improves the read-out characteristics and reduces background noise. The new system that replaced the old scintillation detector (^{6}Li scintillator and an array of 8x8 photomultipliers, **Figure 1**) is characterized by an effective dead-time constant of 25 nsec and an overall count rate as high as 5 MHz at 10% dead-time for flat profiles. These features are due to the fact that the system contains independent channels operated in parallel, which is an advantage over systems that experience dead-time after an event. The much higher count rate shortens the measurement times and therefore increases the number of experiments that can be performed in the same time period.

With all these innovations, the instrument became a highly versatile tool that can address a broad range of structural studies by offering multiple working modes (**Table 2**) that can be selected and used in a direct and user-friendly manner. In the high-intensity mode (**Figure 2B**), up to twelve times the intensity gain compared to the conventional pinhole mode for the same resolution can be achieved with lenses by increasing the sample size. In the tunable resolution mode with chopper and TOF data acquisition, improved characterization of the scattering features within different Q ranges are enabled by the possibility to vary the wavelength resolution $\Delta\lambda/\lambda$ between 2% and 20%[5]. In the extended Q-range mode (**Figure 2C**), using lenses and the secondary high-resolution detector, a Q_m as low as 1×10^{-4} Å^{-1} can be achieved, which, in combination with the pinhole mode, permits the exploration of sizes over a continuous length scale from the nm to the micron range. The use of a chopper for narrowing $\Delta\lambda/\lambda$ provides accurate beam characteristics by avoiding gravity and chromatic effects when using the lenses. In the real-time mode, by exploiting the high intensity and external triggering of data acquisition by sample environments, structural changes can be resolved with time

resolutions down to 50 msec. By improving the wavelength resolution down to $\Delta\lambda/\lambda$= 5% with the chopper, time resolutions as good as 2 msec can be realized.

Here, we present in detail a protocol on how typical experiments are conducted on the KWS-2 in its different working modes and how structural information from the investigated samples can be obtained from the collected data through data reduction. In this demonstration, we will use SANS to characterize several sizes of standard particle solutions and one highly-concentrated polymer micellar solution in order to show how size and order can be studied over broad ranges in a flexible and efficient way with the KWS-2 during one experimental session. Polystyrene spherical particles with different sizes (radii of R = 150, 350, 500, 1,000, and 4,000 Å) and a size polydispersity of $\sigma_R \cong$ 8% are dispersed in a water solution (a mixture of 90% D_2O and 10% H_2O) at a volume fraction of 1%. Micelles formed by the $C_{28}H_{57}$-PEO5 diblock copolymers in D_2O at a concentration of 12% show an ordered structure.

Protocol

1. Loading the Sample Cells

1. Disperse polystyrene spherical particles with different sizes (radii of R = 150, 350, 500, 1,000, and 4,000 Å) and a size polydispersity of $\sigma_R \cong$ 8% in a water solution (a mixture of 90% D_2O and 10% H_2O) at a volume fraction of 1%.
2. Transfer the six solutions of polystyrene particles in D_2O/H_2O, the solution of $C_{28}H_{57}$-PEO5 in D_2O, and the D_2O/H_2O and D_2O solvents to quartz cells (**Figure 3**) using Pasteur pipettes. Fill each of the quartz cells up to the neck. Close the quartz cells with their stoppers.
   NOTE: The operation of filling the quartz cells with samples must be carried out in the sample preparation lab of FRM II by complying with the special working conditions defined there.
3. Install the filled quartz cells into the Al-cartridges of the sample holder (**Figures 3**). Place each filled quartz cell in a cavity of the cartridge and check whether the quartz cell is filled with enough sample by determining whether the sample entirely covers the window opening in the cartridge that is provided for neutrons. Place the correction and the standard samples (the empty quartz cell, the boron-carbide plate, and the Plexiglas plate) in additional locations on the cartridge and leave one location free for the empty beam measurement.
4. Cover the cartridge with the Cd-coated Al-cover plates (**Figure 3**) using cap screws (M3x5). Fix the cartridge on the Al-frame of the sample holder by using the special Al screws (**Figure 4**).

2. Positioning the Sample Holder/Sample Environment on the Sample Stage

1. Determine the necessary space at the sample position of the sample holder by adjusting the length of the collimation nose (**Figure 5**). Select the appropriate configuration for the sample holder from the stored configurations in the collimation nose control system.
2. Install the appropriate sample holder/sample environment on the sample stage in the predetermined position on the optical breadboard using Allen screws, M6x40 (**Figure 6**).
3. Close the motorized sliding lead door (**Figure 5**) by using the knobs on its outer side, keeping the control knobs activated until the door reaches the end position, which will be indicated by a luminous signal.
   Caution: Without the door completely closed and the end-switch activated, the beam shutter cannot be opened, either manually or from the measurement control software; the measurement software will require an additional check for this issue before starting the measurement.

3. Planning the Experiments

1. Choose the adequate experimental configuration and mode for performing the investigation in a *Q* range that is appropriate for the length scale of the structures and the correlation effects revealed by the sample. Check the dynamic range of the instrument[4] (**Figure 7** and **Table 2**).
2. Choose the adequate experimental configuration and mode for enabling proper intensity on the sample based on the estimated level of the scattered intensity by knowing the approximate size, concentration, and contrast factor that characterize the samples to be investigated[8]. This is done in order to optimize the measurement time for a targeted measured statistic and to match the sample stability in case of samples with a short stability time. Check the intensity map for different experimental configurations[4] (**Supplementary Figure 1** and **Table 2**).
3. Choose the adequate experimental configuration and mode for providing a proper resolution based on an approximate knowledge of the degree of polydispersity in size and the concentration of the scattering objects in the sample[8]. This is done in order to enable the resolution of fine scattering features that occur due to ordering effects in the sample. Check for the possibility of tuning the wavelength resolution[5] (**Table 2**).

4. Preparing the Measurement Software and Conducting and Visualizing the Experiment

1. Start the measurement software by typing the KWS2TC in a terminal window at the measurement control computer of the KWS-2 instrument in order to activate the main menu (**Supplementary Figure 3**). Use the left set of functions to define the elementary motor positions (Configuration), to select samples and setup conditions (Definition), to start the measurement and supervise all motors (Control), and to supervise the actual detector (Live-Display).
2. Select the Configuration function in the main menu in order to activate the kws2-Configuration menu (**Supplementary Figure 4**) to define the user data and configure the elementary motor positions and the set-points for the devices and fields on the sample.
   1. Select the UserData function (**Supplementary Figure 4**) and fill the fields User name, E-mail, First part of filename, and Measurement comment in the User data menu (view/edit). Leave the menu by clicking Save.
      Caution: Do not use special characters, like @, $, %, *etc.*, for the file name prefix. Avoid using special characters throughout the entire experimental procedure.

2. Select the Sample function (**Supplementary Figure 4**) in order to activate the Sample configuration menu (**Supplementary Figure 4**). Fill the fields Sample title, Sample beam window - Size, Sample thickness, and Comment for each sample and position selected from the left vertical list of the menu. Save each sample configuration after completing the definition. Leave the menu by clicking Close.
3. Save all configurations under the File function at the upper set of functions in the Configuration menu.

3. Select the Definition function in the main menu (**Supplementary Figure 3**) in order to activate the kws2 Definition menu (**Supplementary Figure 5**) to define the experimental setup and the measurement program.
    1. Select the Sample function in order to activate the Select Samples menu (**Supplementary Figure 5**).
        1. Choose the twelve samples that must be measured (as shown in **Figure 3**) from the list of known samples in the left vertical field and move them to the Selected Samples field using the blue arrow. Order the list of the selected samples by using the blue vertical arrows.
        2. Check the sample parameters and adjust the name, thickness, and comment, if necessary. Leave the menu by clicking Save or Close.

    2. Select the Detector function to activate the Definition of Measurements menu (**Supplementary Figure 6**).
        1. Choose the static measurement type by selecting Standard in the Measurement area. In the End Conditions area, select the proper time unit for the field measuring time.
        2. In the Select Detector and Collimation Distances area, select the experimental setup and working mode by choosing the appropriate values for the wavelength (Selector field), detection distance (Detector Distance field), data acquisition mode (TOF field), aimed wavelength resolution (DLambda/Lambda field), measurement time (Time field), lenses configuration (Lenses field), and collimation distance (Collimation Distance field).
        3. Click the New button after one configuration is entirely defined in order to fix it and store it in the lower table. Define the next configuration and store it in a similar way until the entire set of configurations (**Supplementary Figure 6**) is completed. Hit Save or Close in the Definition of Measurements menu when the adjustment of the experimental setup and working modes is finished.
        4. Sort the list of measurements according to the three loops (sorting conditions) shown at the bottom of the menu that is generated by the program (**Supplementary Figure 7**). Remove the measurements that are not desired by marking the corresponding line and clicking the "X" button marked in red. Adjust the measurement time for each measurement as desired by checking the total defined measurement time in the central field, marked in red, in the kws2 Definition menu, which always remains active on the screen.
        5. Leave the menu with Save or Close and return to the kws2 Definition menu (**Supplementary Figure 5**). Close the kws2 Definition menu and return to the main menu (**Supplementary Figure 3**).

4. Select the Control function in the main menu of the KWS2 measurement software (**Supplementary Figure 3**) in order to activate the Measurement control menu (**Supplementary Figure 8**).
    1. Log in with the username and password that will be communicated by the instrument scientist and lock the session for generating the script, which will execute the commands of the uploaded measurement program. Select Loop Definition in order to check the uploaded measurement program.
    2. Press the Start button and answer the questions generated by the program about the actual status of the sample position door and the beam-shutter. The measurement program will be started. Select Current Values in order to enable the visualization of the ongoing measurement (the positions of motors and the status of instrument components, count rate, and evolution of the integral intensity in time).
    NOTE: The integral intensity on the detector and the count rates of the detector and monitors are shown and can be used to change the measurement program, either individually or the entirety of the set of measurements.

5. Allow the measurements be conducted and completed according to the defined measurement program.
NOTE: The measurements can be interrupted or stopped by activating the Stop function and choosing the desired option (to continue, to stop the current measurement with or without saving the file, or to stop the entire program) when the integral intensity collected up to a certain time point is considered sufficient or when failures are identified in the measurements sequence.
    1. Generate the Logbook of the measurement session by clicking on the Print button under the Loop Definitions option (**Supplementary Figure 8**) when the defined measurement program has been stopped or completed.

6. Select Live-Display in the main menu of the KWS2 measurement software (**Supplementary Figure 3**) in order to activate the KWSlive_MainWindow interface (**Supplementary Figure 9**).
    1. At the Type screen, choose either GEDET or PSD in order to visualize data collected with the main or with the secondary (high-resolution) detector, respectively. Choose the visualization mode at Display Mode by selecting the three-dimensional (Surface), the two-dimensional (Contour), or the one-dimensional (Radial average) mode. Enter the plot options (linear or logarithmic scale) and the parameter values (wavelength and detection distance L_D) in the fields of the Radial average options menu in order to enable the presentation of data as n intensity (uncorrected) versus Q.
    2. Choose a desired TOF-channel in order to visualize the data collected in TOF mode (with either the main or the secondary detector).

5. Data Analysis

1. Start the data processing software by typing the qtiKWS command in a terminal window of the data analysis computer of the KWS-2 instrument. Choose the New Script option on the right side of the main interface.
2. Choose the DAN option in the upper functions menu of the main interface (**Supplementary Figure 10**) in order to activate the data analysis functions. Select the KWS-2 instrument from Options on the right-side menu in order to activate the data analysis mode for data measured on the KWS-2 using the main detector. Define the folder where the measured data files are located and where the corrected data files will be stored.

December 2016 | 118 | e54639 | Page 4 of 23

3. Choose the Tools option and activate the Header(s) function on the right-side menu (**Supplementary Figure 11**) and generate the info-table that contains the files to be processed. Define the table name by clicking the left set of green arrows on the Header(s) field. Load the measured files by clicking the right set of green arrows on the Header(s) field and selecting the measured files.
   NOTE: The info-table that contains the complete information about each measurement file is stored in the explorer-like menu in the lower part of the project. All results that will be generated later in the project will be stored there.

4. Activate the Mask function in the right-side menu (**Supplementary Figure 12**) and generate the active mask that defines the area of the detector that will be considered for data processing. Enter values in the Edge and Beam-Stop fields for defining the lower-left and upper-right corners of the rectangular mask in the case of the analysis of isotropic scattering patterns.

5. Activate the Sensitivity function in the right-side menu (**Supplementary Figure 13**) and generate the detector sensitivity for a certain configuration by entering in the marked green fields the run numbers for the measurements of the standard sample (Plexiglas), empty beam (EB), and blocked beam (B4C).
   1. Click on the set of green arrows next to the yellow field (Transmission) for calculating the transmission of the standard sample. Generate and name the sensitivity matrix by selecting Calculate as New, and visualize the generated matrix by using the appropriate plot functions in the lower menu. Repeat this procedure in case of other configurations.

6. Activate the Data Processing function in the right-side menu (**Supplementary Figure 14**) and generate the correction and calibration table and the script table in order to correct, calibrate, and perform the radial averaging of the data.
   1. Define the number of conditions used in the experiment by using the horizontal slider on the top of the right-side menu (red arrow). Fill the fields indicated with the yellow pencil by entering for each experimental condition the run numbers for the empty cell (EC), blocked beam (B4C), and standard samples-the Plexiglas (Abs. Cal. FS), empty beam for the standard correction (Abs. Cal. EB), and blocked beam for the standard correction (Abs. Cal. B4C).
   2. Enter the run numbers of measurements with strong forward scattering in the Center field. Enter the run number of an empty beam in the EB field and select the corresponding experimental condition for the calculation of the transmission of samples by checking the box next to the Tr (Ec-to-EB) function.
   3. Click each button indicated by a set of rotating green arrows on the vertical series of options (**Supplementary Figure 14**) in order to load the information needed for data processing from the defined files and to calculate the transmission of the empty cell. Click the head of each yellow column in order to define the column name.
   4. Click the New button in order to generate and name the table of the data files that will be processed. Click the Add button in order to load the data files that will be processed. Click the Tr button indicated with the set of rotating green arrows under the Script-Table Tools area in order to calculate the transmission of each sample. Check the results in the generated table (**Supplementary Figure 14**).
   5. Choose Project in the lower-right corner of the interface (**Supplementary Figure 14**) in order to save all results as tables or matrices in the current qtiKWS session (project). Click the I[x,y] button in order to perform the correction and calibration of two-dimensional data. Click the I(Q) button in order to perform the correction, calibration, and radial averaging of the data. Plot the results using the graphical functions under the Graph (**Supplementary Figure 15**) option.
   NOTE: All results will be generated as external files that will be saved in the external folder that was defined in step 5.2, when, in the lower-right corner of the interface, File is chosen instead of Project.

7. Chose Tools in the right-side menu (**Supplementary Figure 11**) and activate the TOF|RT option (**Supplementary Figure 16**) in order to split the data that were collected with the main detector in the TOF working mode into single files corresponding to each time channel.
   1. Click the TOF :: Calculate Parameters function and load one file, from which information about the TOF conditions is extracted. Click on the TOF|RT :: Sum vs Number :: Read function and load the file of interest, measured in real-time or TOF modes, in order to generate a sum-tof-file table like that shown on the left side of the working interface. Plot the integral intensity as a function of time channels (**Supplementary Figure 16**) from the sum-tof-file using the graphical options under the Graph function in the upper functions menu.
   2. Define the processing parameters in the fields of the TOF function. Click the TOF|RT :: All Selected Steps :: Proceed button in order to load the data files that will be separated into single files corresponding to each of the defined time slots.
   NOTE: Files that contains data measured in every time slot are generated and stored in the file location defined in step 5.2 and receive the name of the original TOF file, followed by the number of the time slot.
   3. Proceed as in step 5.6 in order to analyze the data measured with improved resolution, corresponding to $\Delta\lambda/\lambda_{aimed}$, using the chopper.

8. Select the KWS2-HRD instrument from Options on the right-side menu of the main interface (**Supplementary Figure 17**) in order to activate the data analysis mode for data measured with the KWS-2 using the secondary high-resolution detector. Activate the Mask function in the right-side menu (**Supplementary Figure 18A**) and generate the active mask that defines the active area of the detector.
   1. Choose the DANP option in the upper functions menu of the main interface (**Supplementary Figure 18B**). Select the ASCII.2D option in the right-side menu. Activate the 2D Masking function in order to define a special sector on the detector that will be considered for the data analysis.
   2. Introduce the beam-stop center in the field Center. Select the mask matrix and the value 0 in Mask :: Conditions to neglect the outside area of the special mask. Choose the angular sector and click the colored button on the right side of the sector fields. Proceed with the data measured with the high resolution detector, as in steps 5.5 and 5.6.

9. Save the qtiKWS project (save functions under the File option of the upper menu).

Representative Results

Representative results of a successful experiment that was carried out with the KWS-2 in different working modes on the structure and morphology of two representative types of soft matter systems are given in **Figures 8-11**. These results are from the investigation of a series of polystyrene standard-size particles in D_2O/H_2O solutions, with a D_2O content of 90%, and of the fully-protonated diblock copolymer $C_{28}H_{57}$-PEO5 in D_2O at a high polymer volume fraction (12%). The polystyrene standard-size particles, with radii of R = 150, 350, 500, and 1,000 Å were used to test the conventional pinhole mode using different combinations of detection distances L_D and wavelengths λ. Larger-sized particles (R = 4,000 Å) were used to test and commission the extended Q-range mode. The diblock copolymer that yields an ordered micellar structure at high concentrations of D_2O was used to test and commission the tunable resolution mode.

Figure 8 presents the results of the two-dimensional scattering patterns measured in pinhole mode using the main detector (the old scintillation detector) and in the extended Q-range mode using the focusing lenses and the high-resolution secondary detector. **Figure 8A** represents the scattering pattern from polystyrene particles with R = 500 Å measured at L_D = 8 m by using λ=5 Å. **Figure 8B** shows the scattering pattern from polystyrene particles with R = 1,000 Å, collected at L_D = 20 m by using λ= 20 Å. For the measurements performed with λ = 5 Å, the direct beam was collected on the central beam-stop installed in front of the detector, and the transmitted beam could be monitored with a small ³He counter that was installed in the middle of the beam-stop. This is the so called Monitor 3 (**Supplementary Figure 8**). The instrument has two additional ³He counters, which are installed in front of the velocity selector (Monitor 1) to monitor the polychromatic beam, and behind the velocity selector (Monitor 2) to monitor the monochromatic beam. Due to technical limitations, the measurements with λ = 20 Å were performed with the direct beam on the detector, which was the typical setup used with the old KWS-2 detector. The weaker, direct beam intensity at long wavelengths, which drops down due to gravity, could be detected without damage caused to the detector. The transmitted beam in this case was monitored with Monitor 3 at a short detection distance L_D = 2 m. In this case, the gravity effects are weak and the direct beam falls on the beam-stop (like in the **Figure 8A**). The data collected two-dimensionally on the detector for a pixel size of 5.25 mm x 5.25 mm were further corrected for the detector sensitivity, and the contributions from the empty cell, instrument background, and solvent were absolutely calibrated using the scattering from the Plexiglas secondary standard[4]. Finally, the scattering patterns that were isotropically distributed around the position $Q{\rightarrow}0$ were averaged radially, which delivered the dΣ/dΩ for each polystyrene particle system.

The two-dimensional scattering pattern from the large polystyrene particles (R = 4,000 Å) is shown in **Figure 8C**, as it was measured with the high resolution detector for a pixel size of 0.5 mm x 0.5 mm. The small direct beam is focused by the lens system on the detection plan and is captured by a small beam-stop (4 mm x 4 mm) installed on the detector face. The shadow from the quadratic beam-stop can be observed in **Figure 8C** in the upper-left side of the active detector area. The gravity effects induce a wide vertical distribution of neutrons of different wavelengths on the detector. Additionally, because the lenses are focused perfectly, only the neutrons characterized by the central wavelength λ of the triangular distribution are delivered by the velocity selector[2,5]; the neutrons of different wavelengths around the central one arrive on the detector slightly out of focus. These two effects yield the weak direct beam traces that can be observed just above and below the beam-stop. In the static extended Q-range mode using lenses and the high-resolution detector, the data are collected continuously. In order to diminish the contribution of gravity effects, the scattered data are analyzed in a narrow angular sector that starts from the beam-stop and stretches horizontally to its right, as depicted in **Figure 8C**. The data are processed further using the typical approach for achieving the dΣ/dΩ. **Figure 8D** presents the intensity versus the position from the beam-stop towards the rim of the detector, as it was collected in a narrow horizontal slice with a width of 1 pixel (0.5 mm) on the high resolution detector. Data from the sample solution and the reference (solvent) are shown as they were collected in a short test measurement of 5 min. The drop of intensity at short positions is due to the beam-stop. From the ratio of the intensities at the shortest positions, the sample transmission (87%) could be estimated.

The corrected and calibrated results obtained in terms of dΣ/dΩ on the solution of the polystyrene particles with R = 500 Å are shown in **Figure 9**, together with those from the solvent. These results illustrate the Q range that can be covered with the KWS-2 in conventional pinhole mode through the variation of the detection position L_D and the use of one or more wavelengths. The form factor features[8,9] of the spherical particles are also revealed: the Guinier region at low Q and the oscillations due to the spherical Bessel function in the intermediate Q range. In the high Q range, the scattering profile is dominated by the scattering from the solvent, and therefore it shows a flat behavior, like that from the solvent itself. The form factor minima are affected by the instrument resolution[5] on the one hand, and by the particle size polydispersity on the other hand. The instrument resolution in the case of the KWS-2 is mostly determined by the wavelength spread of Δλ/λ= 20%. The size polydispersity for all types of particles was about σ_R = 8%. **Figure 10** shows the results obtained in the SANS investigation of all types of polystyrene particles expressed as dΣ/dΩ after the correction for the solvent contribution was applied. The Guinier regions are clearly evidenced for all particles towards low Q values, while in the high Q ranges, the slope of -4 is revealed, which is typical for the form factor of the spherical objects. The structural parameters of the standard-size particles were confirmed by the fit of the data with the form-factor of polydisperse spheres[8,9] convoluted with the resolution function of the instrument[10-12].

Figure 11 presents the two-dimensional and the radially-averaged one-dimensional scattering patterns from the ordering structure of $C_{28}H_{57}$-PEO5 polymer micelles that occurs in D_2O at a polymer volume fraction of 12%. The results were collected at different detection distances L_D, with both conventional pinhole and tunable resolution modes combined in the same measurement session. When the system is investigated in the conventional pinhole mode using the wavelength spread of Δλ/λ= 20%, as provided by the velocity selector, and continuous (static) data acquisition, three broad peaks are observed in the scattering patterns at L_D = 4 m. In the tunable resolution mode, by using the chopper and the TOF data acquisition in combination with the velocity selector, the wavelength spread can be improved so that it can be checked whether these features are real or if a fine structure of them will eventually appear. The first and second peaks observed at Δλ/λ= 20% reveal a splitting when they are measured with Δλ/λ= 5%, which enabled the clear identification of the ordering of micelles into face-centered cubic (fcc) crystals[5,13].

These are two typical examples of how the versatility and performance of the KWS-2 SANS diffractometer can be used in an easy and user-friendly way by following the provided protocol for conducting detailed investigations on soft matter and biophysical systems that show complex structural features in terms of length scale and ordering.
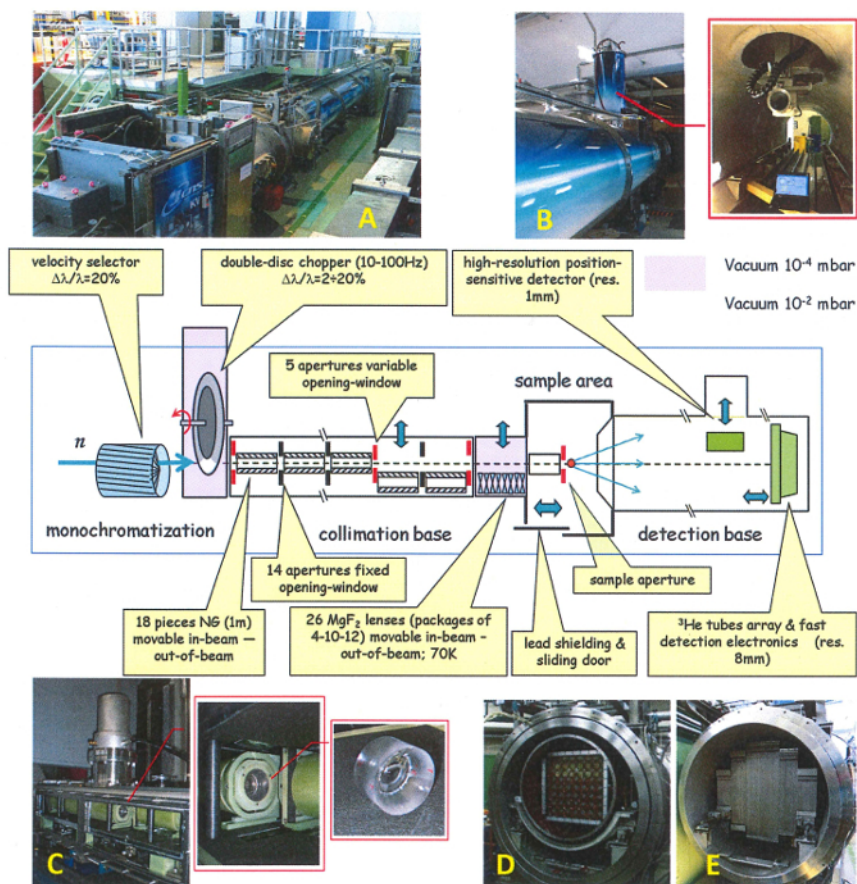
Figure 1: Layout of the KWS-2 SANS instrument, including all upgrades done between 2010 and 2015. (**A**) The general view of the instrument. (**B**) The secondary high-resolution detector and its tower on the top of the vacuum tank. (**C**) The MgF_2 focusing lenses, grouped into three packages, and their cooling system (cold head). (**D**) The old main detector (scintillation) with its 8 x 8 array of photomultipliers. (**E**) The new main detector (^{3}He tubes) with a larger detection area. Please click here to view a larger version of this figure.
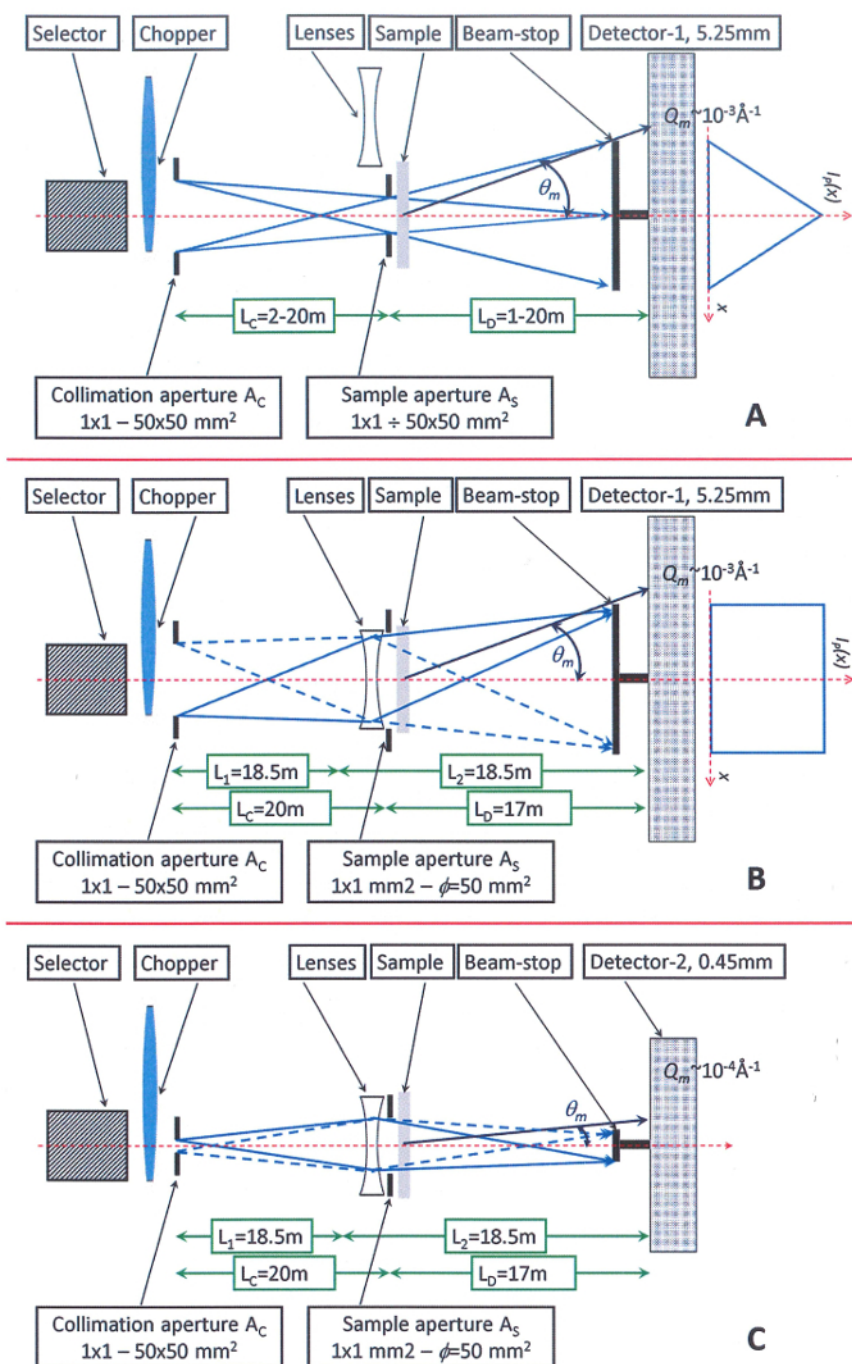
Figure 2: Schematic view of three working modes offered on the KWS-2. (A) The conventional pinhole mode. For $L_C = L_D$, where L_C and L_D are the collimation and the detection length, respectively, and optimal pinhole condition $A_C = 2A_S$, where A_C and A_S are the collimation entrance aperture and the sample aperture, respectively, the beam profile I'_P at the detector is approximately triangular with a base width equal to $2A_C$. **(B)** The high-intensity focusing mode. By using lenses, larger samples can be measured with the same resolution as in the conventional pinhole mode (the beam profile I'_P at the detector is rectangular in this case). **(C)** The extended Q-range focusing mode. By using lenses and a small entrance aperture A_C (typically 4 mm x 4 mm) that is placed on one focal point of the lens system, a small beam is transmitted onto the detector, which is placed on the other focal point of the lenses. Hence, a lower value for the minimum wave vector transfer Q_m than in conventional pinhole mode can be achieved. Please click here to view a larger version of this figure.
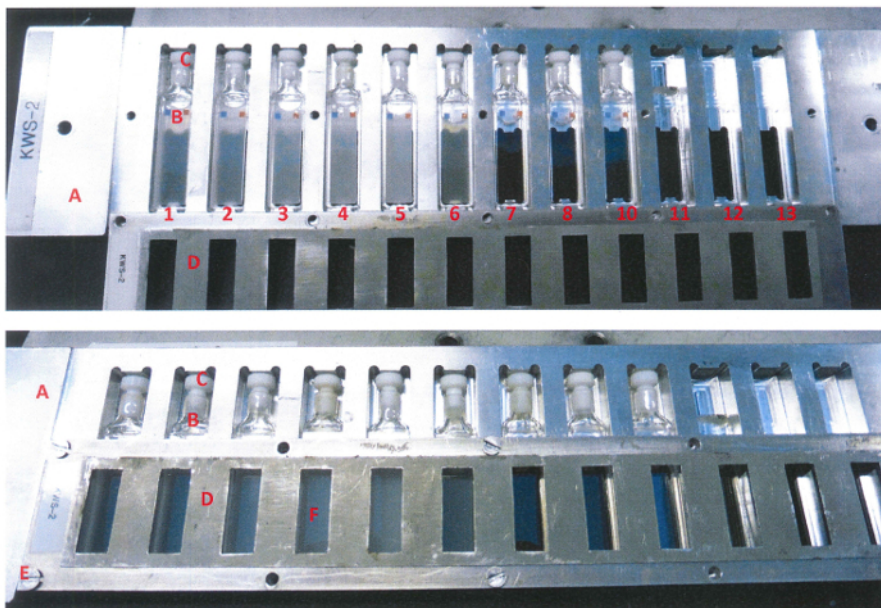
**Figure 3: View of the samples mounted in the Al-cartridge of the sample holder for measurements at ambient temperature. In the cavities provided in the Al-cartridge.** (**A**) quartz cells (**B**) filled with samples and covered with their stoppers (**C**) can be placed. The positions on the Al-cartridge were occupied with samples as follows: in positions No. 1 to No. 5, the polystyrene particles with sizes of R = 150, 350, 500, 1,000, and 4,000 Å in D_2O/H_2O solvent; in position No. 6, the $C_{28}H_{57}$-PEO5 diblock copolymer in D_2O; in positions No. 7 and No. 8, the solvents D_2O/H_2O and D_2O; in position No. 9, the empty quartz cell (reference); in position No. 10, the Plexiglas (standard); in position No. 11, nothing (for the measurement of the empty beam); in position No. 12, the B_4C plate (taped on the back side; for the measurement of the instrument background with the blocked beam). The Al cover plate (**D**), coated with Cd mask on the outer face, is fixed on the top of the cartridge with the screws (**E**) in order to secure the sample cells and to define the neutron window (**F**). Please click here to view a larger version of this figure.
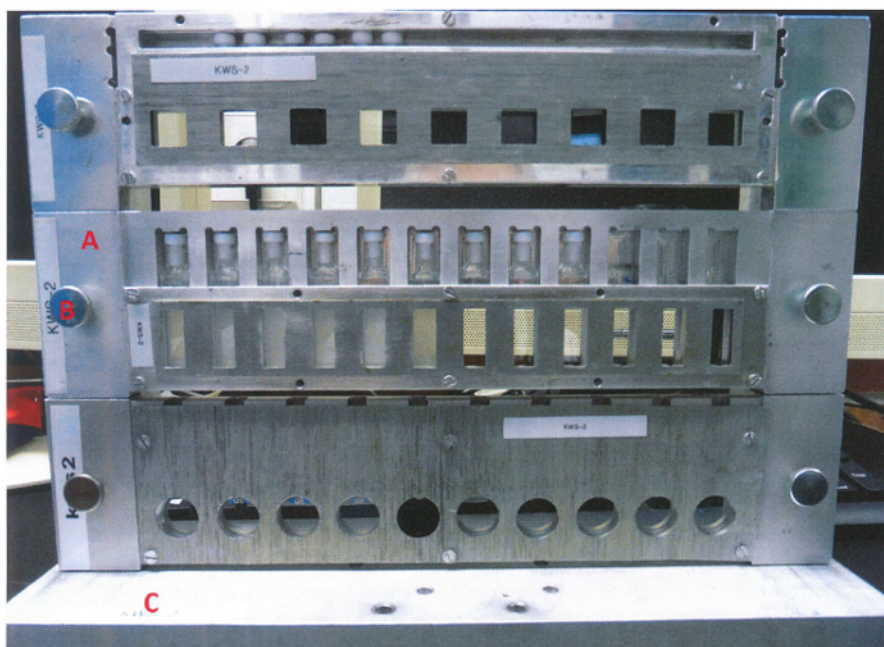

Figure 4: View of one of the multilevel and multi-position cell-holders used on the KWS-2 for measurements at ambient conditions. The samples for the current experimental session were installed in the middle level. The three levels can be equipped with cartridges (**A**) designed for different cell geometries that are closed with Al-cover plates coated with Cd masks on the outer face (towards the neutrons). The installation of the cartridges on the holder is done using the screws (**B**). The holder has a base support (**C**) which allows its installation in a predetermined position on the sample stage. Please click here to view a larger version of this figure.
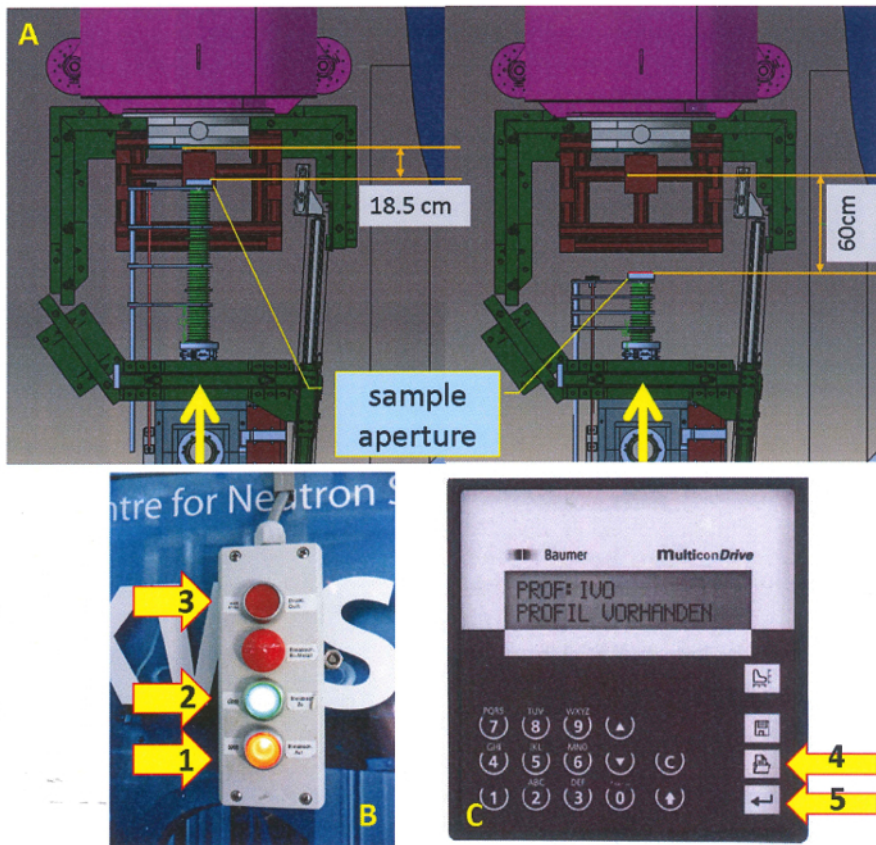
Figure 5: Schematic top view of the sample area of KWS-2. (**A**) Presentation of two extreme configurations of the collimation nose, showing the available space for the installation of various sample environments in beam (the neutrons are coming from the bottom, as indicated by the yellow arrows). (**B**) The control panel of the lead door, with the opening and closing keys (1 and 2, respectively). The door motor works only as long as the keys are continuously pressed. The door is equipped on its edges with sensors that induce the shutdown of the motor when an obstacle is sensed. After removing the obstacle, the motor blocking can be canceled with the upper key (3) and the opening or closing action can be resumed. (**C**) The control panel of the collimation nose. From the nose panel, an appropriate configuration can be selected using the key (4). The nose is moved by keeping the key (5) continuously activated until the selected positioning is reached and the movement stops by itself. Please click here to view a larger version of this figure.
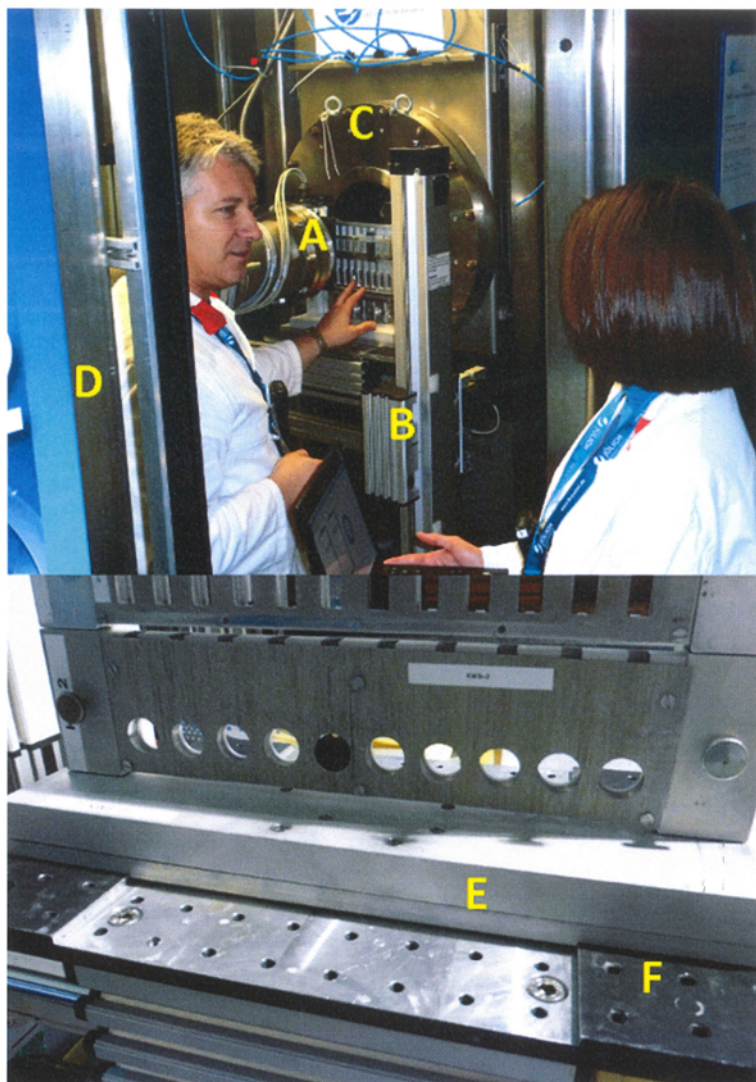
Figure 6: Installation of the multilevel and multi-position sample holder on the sample stage for SANS measurements at ambient temperature (Photo credits: Wenzel Schürmann, Technische Universität München, Germany). The main components at the sample position are the collimation nose with the sample aperture at its end (**A**), the sample stage that provides the horizontal and vertical positioning of the samples in the beam (**B**), the entrance window of the detector vacuum tank (**C**), the lead door with sensors on its edge (**D**), and the base support of the cell holder (**E**), which provides for the installation of the holder on the optical breadboard (**F**) of the sample stage. Please click here to view a larger version of this figure.
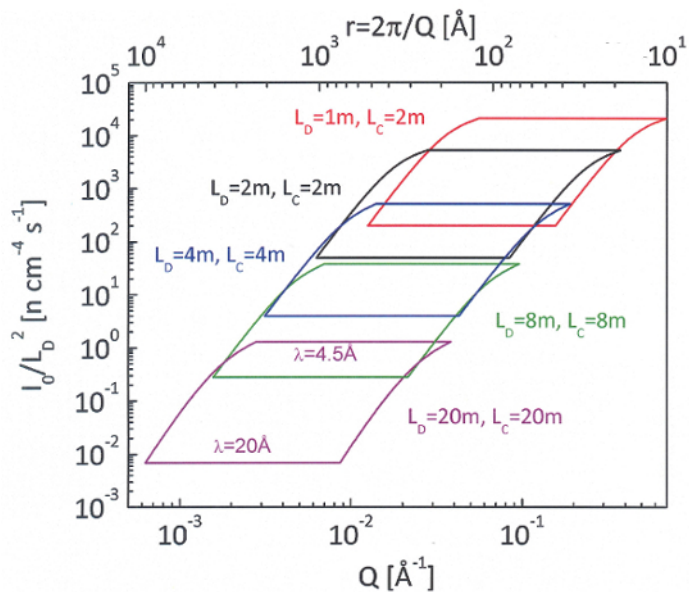
Figure 7: The dynamic range for different instrumental setups on the KWS-2. I_0 represents the neutron flux at the sample position. The defined areas indicate the available Q range that can be covered when the wavelength is varied between 4.5 Å and 20 Å for particular collimation-detection configurations. Please click here to view a larger version of this figure.
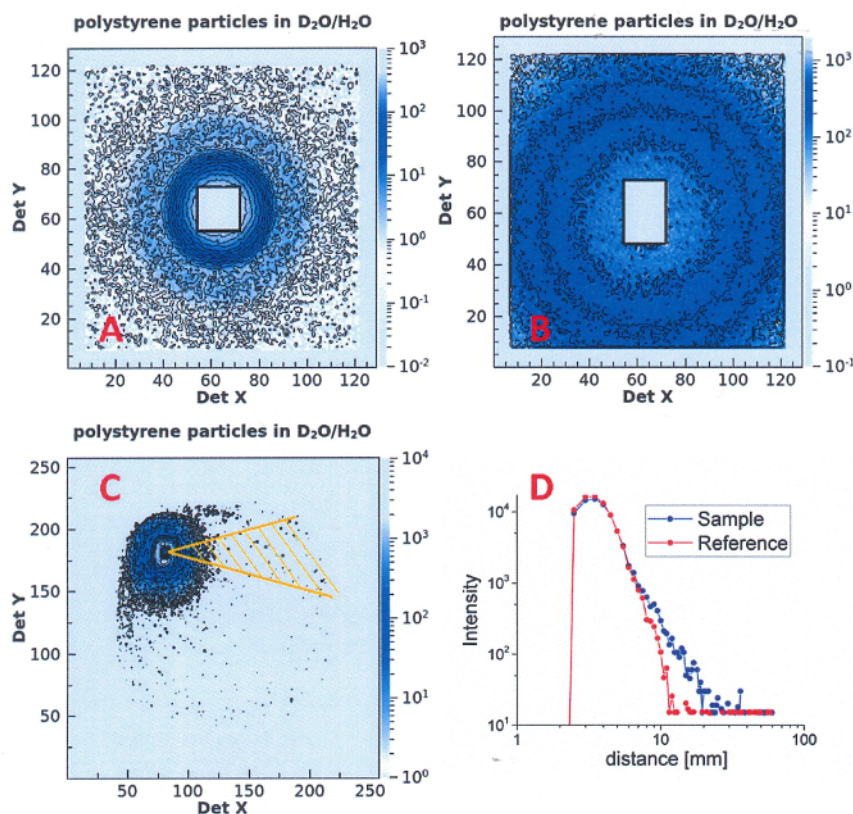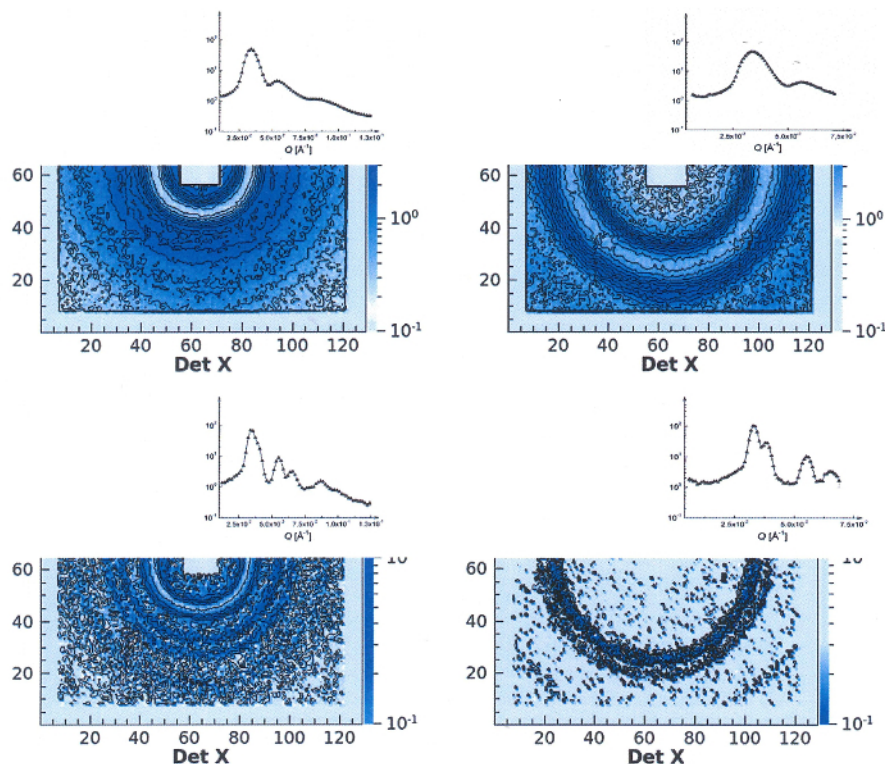
Figure 8: Examples of two-dimensional scattering patterns collected during the experimental session according to the current protocol. (**A**) The scattering pattern collected at L_D = 8 m from polystyrene particles with a radius of R = 500 Å in D_2O/H_2O, as measured with λ= 5 Å. The scattering pattern is isotropically distributed around the beam-stop, which is blocking the direct beam in the middle of the detector. (**B**) The scattering pattern collected at L_D = 20 m from polystyrene particles with a radius of R = 1,000 Å in D_2O/H_2O, as measured with λ= 20 Å. The scattering pattern is isotropically distributed around the position of the transmitted beam, which for this wavelength falls under the beam-stop and is masked together with the beam-stop using the functions of the visualization software. (**C**) The scattering pattern collected with the high resolution detector at L_D = 17 m from polystyrene particles with a size of R = 4,000 Å in D_2O/H_2O, as measured with λ= 7 Å in the extended Q range, with lenses and the high resolution detector. The scattering pattern is isotropically distributed around the small beam-stop (4 mm x 4 mm), which blocks the focused direct beam. The angular sector in which the data are further analyzed is indicated on the right side of the beam-stop. (**D**) The intensity versus the position from the beam-stop as it was collected in a short test measurement in a narrow horizontal slice, with the width of 1 pixel (0.5 mm), on the high resolution detector. The data are shown from the sample solution and the reference (solvent). Please click here to view a larger version of this figure.
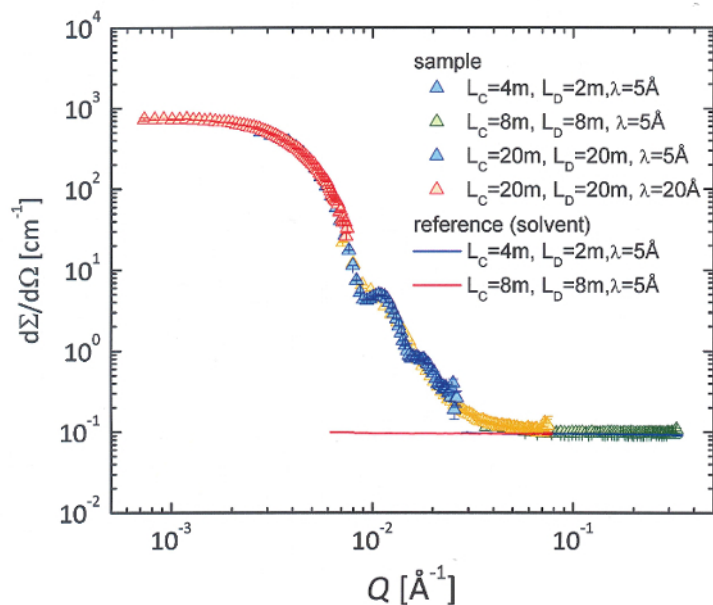
Figure 9: The scattering patterns from the polystyrene particles in D_2O/H_2O solution (symbols) and from the solvent (lines). The data were collected in the conventional pinhole mode at different instrument configurations that are indicated by different colors. Please click here to view a larger version of this figure.
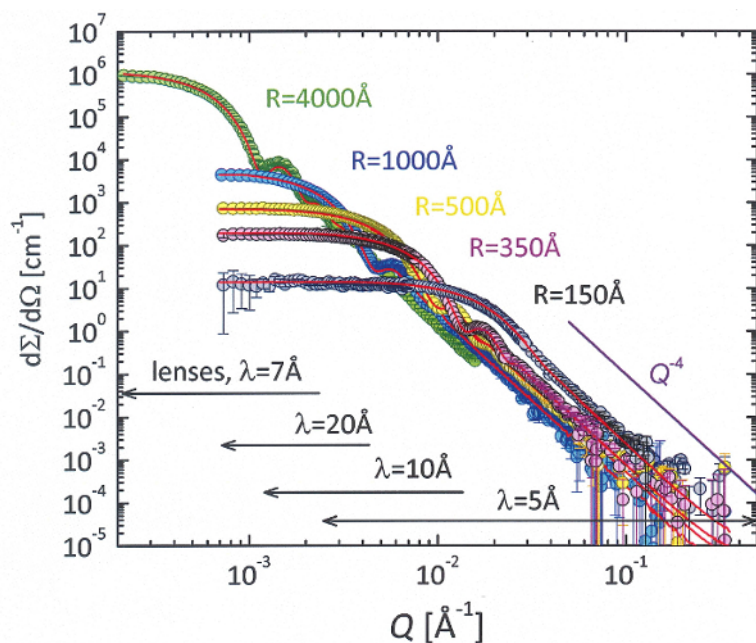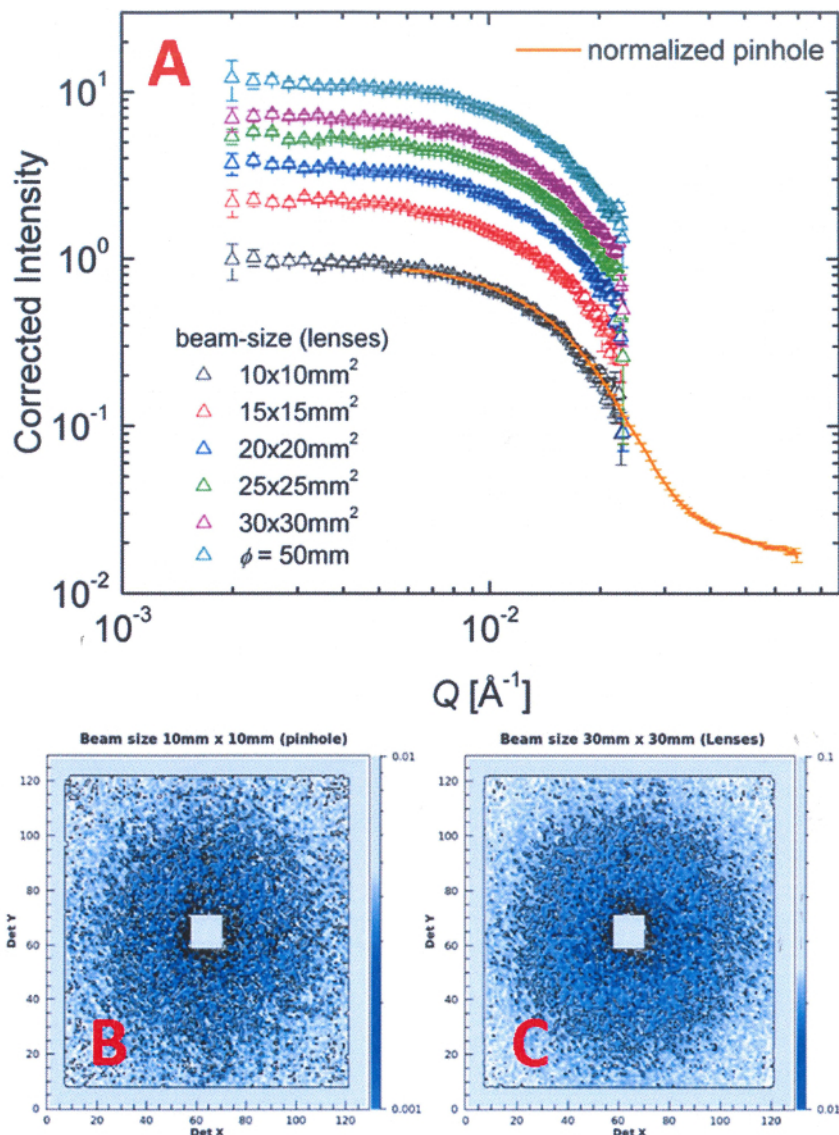

Figure 10: The scattering patterns from polystyrene particles of different sizes in D_2O/H_2O after the correction for the scattering from solvent was applied. The red lines represent fits with the spherical form-factor[9], including the instrument resolution[10, 11] and the size polydispersity. The typical Q^{-4} asymptotic behavior for the spherical form factor is indicated by the straight line in the high Q range. The low limit of the Q range covered with different wavelengths or setups is specifically marked. Please click here to view a larger version of this figure.

Figure 11: The two-dimensional and the radially averaged one-dimensional scattering patterns from the $C_{28}H_{57}$-PEO5k polymer micelles in D_2O (at a polymer volume fraction of 12%), measured in the conventional pinhole mode with Δλ/λ= 20% (top) and in the tunable resolution mode, with Δλ/λ= 5% at L_D = 4m (left side) and L_D = 8m (right side). In the conventional mode, three broad peaks could be observed. A fine structure of the first two peaks is revealed[5, 13] with improved Δλ/λ resolution. Please click here to view a larger version of this figure.
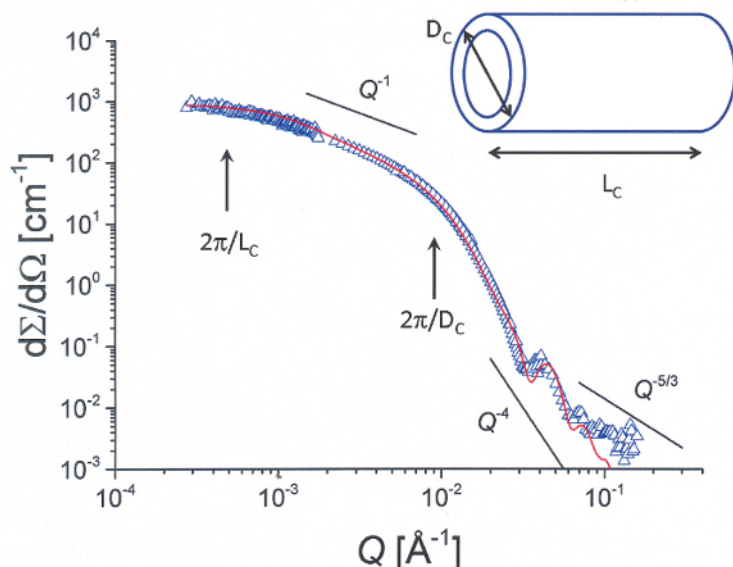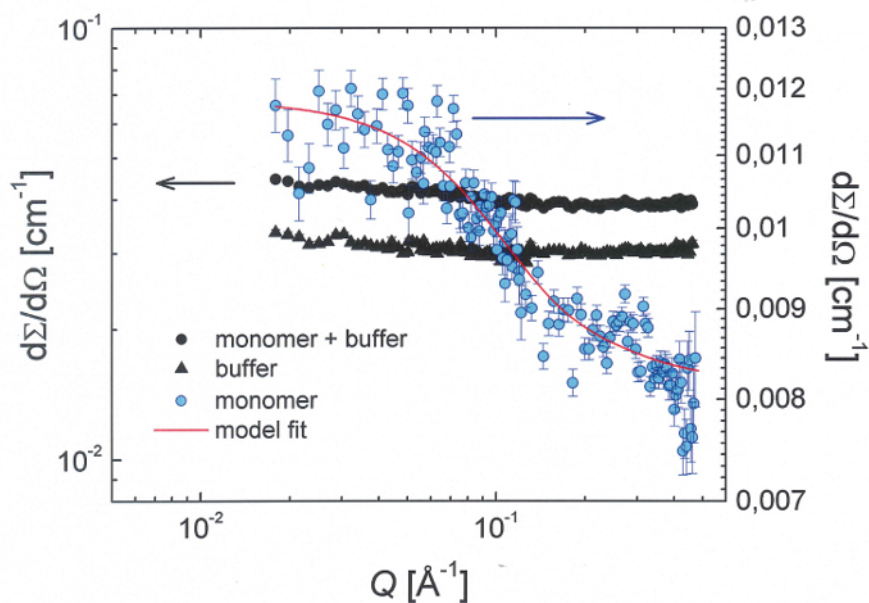

Figure 12: The scattering pattern from fully-protonated PHO10k-PEO10k diblock copolymer micelles in D_2O (after the correction for the scattering from solvent was applied), as measured by combining the conventional pinhole and the extended Q-range modes. A core-shell cylindrical morphology is indicated by the Q^{-1} dependence of scattered intensity at intermediate Q and the $Q^{-5/3}$ dependence (blob scattering) observed at high Q. The intensity plateau at low Q and the bending at intermediate Q reveal the length and the thickness of the cylinders, respectively. The red curve represents the fit of the experimental data with a core-shell cylinder model[9], with the instrumental resolution included[10-12]. Please click here to view a larger version of this figure.
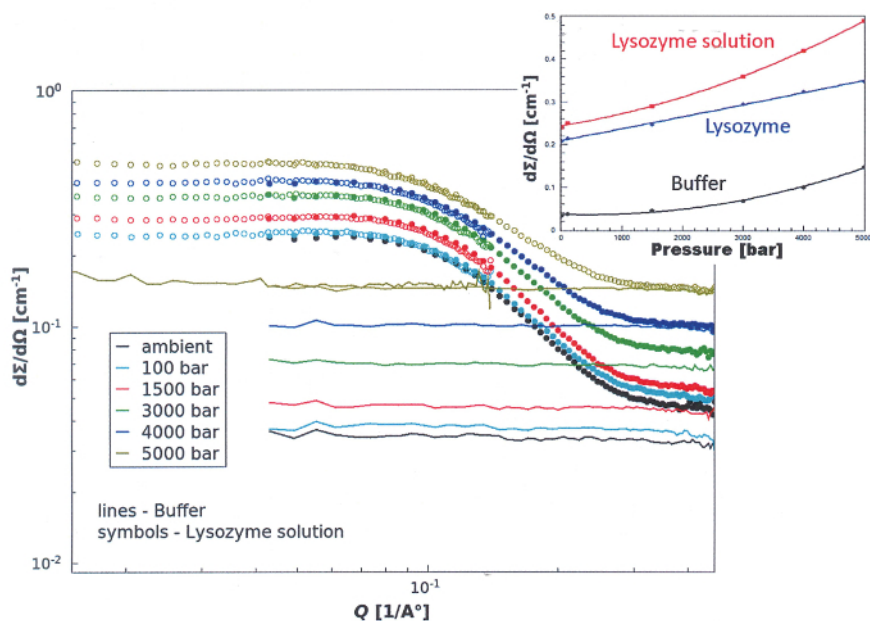
Figure 13: The scattering patterns from polystyrene particles (R = 150 Å) in D_2O/H_2O, as measured in the conventional pinhole and high-intensity (lens) modes. (**A**) The one-dimensional scattering patterns measured with λ = 7 Å at L_D = 8 m in the conventional mode and at L_D = 20 m in the high-intensity mode with lenses. In the high-intensity mode, different beam sizes on the sample were used in order to increase the intensity. Up to 12 times the gain in intensity was achieved when 26 lenses were used compared to the conventional pinhole mode. A large sample was placed in the beam by using a round quartz cell with a diameter of 5 cm. (**B**) The two-dimensional scattering pattern collected on the detector in pinhole mode for a beam-size of 10 mm x 10 mm. (**C**) The two-dimensional scattering pattern collected on the detector in high-intensity mode by using 27 lenses and a beam size of 30 mm x 30 mm. The size (resolution) of the direct beam focused on the detector is the same as in the pinhole mode. Please click here to view a larger version of this figure.

Figure 14: The scattering pattern from the buffer solution and from the beta amyloid protein monomers (Aβ 1-42, molecular weight M_W = 4.5 kDa) in deuterated hexafluoroisopropanol dHFIP buffer at a concentration of 5.6 mg/ml after three weeks of incubation. The full dots represent the scattering curve from the protein solution while the full triangle shows the scattering curve from the buffer solution. The blue dots denote the scattering cross-section (on the right vertical scale) from monomers after the correction for the buffer contribution was applied. The error bars represent the standard deviations derived from the neutron counts. The red solid line shows the fitted Beaucage function with fixed dimensionality d=2[14]. Please click here to view a larger version of this figure.

Figure 15: The scattering patterns from lysozyme 50 mg/ml in 50 mM acetate buffer in D_2O and from buffer solution measured at different pressures, from ambient to 5,000 bar. The symbols represent data from the protein solution while the lines show the data from the buffer. The data was collected at two detection distances, L_D = 4 m (open symbols) and L_D = 1 m (full symbols). The inset shows the behavior of the forward scattered intensity I($Q{\rightarrow}0$) from the protein solution, the buffer, and the protein itself (after the correction for the buffer contribution was applied) as a function of pressure. Please click here to view a larger version of this figure.

Parameter / Function	Ancillary equipment	Range of use	Accuracy	Technical Details
Positioning	Sample stage			max. load 600 kg
	X	0 - 360 mm	0.05 mm	
	Y	0 - 330 mm	0.05 mm	
	Z (beam axis)	manually, 600 mm		
	θ_r (rotation)	0° - 360°	0.002°	
	θ_t (cradle)	± 30°	0.002°	
Ambient temperature	three-level multi-position Al holder (Cd masks)			3x9=27 wide quartz cells
				3x12=36 narrow quartz cells
	three positions			3 large quartz cells (diameter Φ = 5 cm)
	Al holder (B$_4$C mask)			
Temperature	thermostat (oil bath) +	from -25 °C to 200 °C	± 0.5 °C	4 positions
	small copper block			in air or in vacuum chamber (with sealed cuvettes)
	thermostat (water bath) + two-level multi-position	from 5 °C to 85 °C	± 0.2 °C	2x9=18 wide quartz cells; 2x12=24 narrow quartz cells
	Al block			
	thermostat + high precision oven	from 10 °C to 120 °C	< 0.1 °C	1 position, wide quartz cell
	Peltier-thermostated cuvette-holder	from -20 °C to 140 °C	± 0.2 °C	8 positions (all types of quartz or bras sandwich type cells cells); controlled atmosphere below 5 °C
	(B4C mask)			
Pressure	HP cell SANS + thermostat (water bath)	up to 5,000 bar		Temperature in the range from 5 °C to 85 °C
Low-temperature	Cryostat with sapphire windows	down to 50 K		
Rheometry	Rheometer; steady state and oscillatory modes			
Humidity	Humidity Cell	5% to 95%		Temperature in the range from 15 °C to 60 °C
In-situ FT-IR[20]	FT-IR spectrometer			Sample cells with ZnSe windows

Table 1: The list of ancillary equipment available for the KWS-2 SANS diffractometer, including the range of use, the accuracy, and the details of each device.

December 2016 | 118 | e54639 | Page 18 of 23

Measurement Mode	Experimental setup	Resolution	beam/sample size	max. intensity [n/s]	Q-range [Å^{-1}]
		$\Delta\lambda/\lambda$			
Conventional pinhole	λ = 7 Å	20%	10 x 10 mm^2	1.3 x 10^8	0.002 .. 0.3
	L_C = 2 m - 20 m				
	L_D = 1 m - 20 m				
	λ = 4.5 Å, L_C = 2 m, L_D = 1 m	20%	10 x 10 mm^2	2 x 10^8	0.01 .. 0.5
	λ = 10 Å, L_C = 20 m, L_D = 20 m	20%	10 x 10 mm^2	7.5 x 10^5	0.001 .. 0.02
	λ = 20 Å, L_C = 20 m, L_D = 20 m	20%	10 x 10 mm^2	4 x 10^4	7x10^{-4} .. 1.5x10^{-2}
Focusing high-intensity	λ = 7 Å, L_C = 20 m, L_D = 17 m	20%	Φ = 50 mm	3 x 10^7	$\approx$ 0.002 .. 0.03
Focusing high-resolution (extended Q-range)	λ = 7 Å, L_C = 20 m, L_D = 17 m, A_C = 4 x 4 mm^2	20%	10 x 10 mm^2	1.6 x 10^4	$\approx$ 2x10^{-4} .. 0.02
Tunable resolution	λ = 4.5 Å,	5%	10 x 10 mm^2	*ca.* 7% from conventional mode	0.002 .. 0.5
	L_C = 20 m,				
	L_D = 1 m .. 20 m				

Table 2: The experimental configurations available on the KWS-2 SANS diffractometer.

Supplementary Figure 1: The absolute neutron flux at the sample position of the KWS-2 as a function of wavelength λ at different collimation lengths L_C and for optimal filling of the reactor cold source. Please click here to download this figure.

Supplementary Figure 2: Schematic view of the double disc chopper with a variable slit opening. The slit opening $\Delta\varphi$ can be adjusted between 0° and 90° so that, depending on the chopper frequency $f_{chopper}$, the opening time τ_w of the guide (the red rectangle on the right vertical series of pictures) can be varied. Please click here to download this figure.

Supplementary Figure 3: The main user interface of the measurement control and visualization software of the KWS-2. The left-side functions (**A**) can be used by experimentalists, while the right-side functions and indicators (**B**) are used by the instrument responsible. A server or process shown in the right-side menu is operational and works normally when it is marked in green. The components marked in yellow are not activated. Any malfunction is indicated with red. Please click here to download this figure.

Supplementary Figure 4: View of the kws2-Configuration menu and Sample configuration functions. The users must fill in information in the UserData fields first and then do the configuration of samples. The fields that must be filled and the actions that must be taken are marked in red. Please click here to download this figure.

Supplementary Figure 5: View of the kws2 Definition menu and Select Sample functions. The actions that must be taken by the user are described in step 4.3. Please click here to download this figure.

Supplementary Figure 6: View of the kws2 Definition menu and Definition of Measurements functions. The actions that must be taken by the user are described in step 4.3. Please click here to download this figure.

Supplementary Figure 7: The measurement program generated by combining the defined samples and the defined experimental conditions. The actions that must be taken by the user are described in step 4.3. Please click here to download this figure.

Supplementary Figure 8: The kws2-Measurement control menu and the Current Values option. The fixed parameters (positions, names, wavelength, *etc.*) and the variables (time, intensities, count rate, *etc.*) that characterize the running measurement are displayed. The actions that must be taken by the user are described in step 4.4. Please click here to download this figure.

Supplementary Figure 9: The Live-Display option with the KWSlive_MainWindow menu and different data visualization options. The Surface visualization mode is selected. When the Radial average mode is selected (right-side image), the setting of parameters can be found under the Options menu Please click here to download this figure.

Supplementary Figure 10: The main interface of the data reduction software qtiKWS with the options for the selection of the instrument and the location of the experimental and processed data. Please click here to download this figure.

Supplementary Figure 11: The functions for defining the log-book for the set of data to be treated (info-table). The actions that must be taken by the user are described in step 5.3. Please click here to download this figure.

Supplementary Figure 12: The functions for defining the detector mask for which the data will be processed. The actions that must be taken by the user are described in step 5.4. Please click here to download this figure.

Supplementary Figure 13: The functions for defining the detector sensitivity maps. The actions that must be taken by the user are described in step 5.5. Please click here to download this figure.

Supplementary Figure 14: The functions for generating the script table for the correction, calibration, and radial averaging of data. The actions that must be taken by the user are described in step 5.6. Please click here to download this figure.

Supplementary Figure 15: The functions for plotting the processed data. The actions that must be taken by the user are described in step 5.6.5. Please click here to download this figure.

Supplementary Figure 16: The functions for the preparation and splitting of the data measured in the tunable-resolution mode. The data from the two pulses delivered by the chopper and collected initially in 64 TOF channels are merged into one pulse. Several channels are grouped together so that the resulting time channels that are characterized by the $\Delta\lambda/\lambda_{aimed}$ can be saved as separate files. Please click here to download this figure.

Supplementary Figure 17: The main interface of the data reduction software qtiKWS with the selected option for processing the data measured with the high-resolution detector. Please click here to download this figure.

Supplementary Figure 18: The functions for defining the high-resolution detector masks for which the data will be processed. The actions that must be taken by the user are described in step 5.8. Please click here to download this figure.

Supplementary Figure 19: Overview of all types of sample cells typically used on the KWS-2 for the investigation of soft matter and biological samples at ambient or variable temperature. (A) View of the large quartz cells available for the high-intensity mode with lenses and a large beam size. The cell holder, which is equipped with borated plastic masks (1), permits the planning and conducting of three measurements in one session. (B) View of the quartz or brass cells that are used as sample containers and of a temperature controlled holder (Peltier-type) equipped with 8-position cartridges appropriate for each type cell. The holder is shielded with borated plastic masks (1) on both faces. (C) View of the pressure cell in operation on the KWS-2. The cell can provide pressure on the sample between the ambient and 5,000 bar in an automatic mode, controlled by the measurement program. The round Cd mask (1) with a small aperture in the middle determines the beam-size on the sample. Please click here to download this figure.

Discussion

Soft matter and biophysical systems are typically characterized by structural correlations and interrelated microstructural and morphological levels that span a wide length scale, from nm to microns. To understand the mechanism of formation and evolution of the morphology of such systems and the relationship between their microscopic features and macroscopic properties, it is important to explore their microstructure over the entire length scale and under relevant environmental conditions (*e.g.,* temperature, pressure, pH, humidity, *etc.*). Typically, small-angle scattering techniques with neutrons (SANS) or synchrotron X-rays (SAXS) are involved in such studies. The intensity drawback of neutrons versus synchrotron X-rays is compensated by the use of comparatively large $\Delta\lambda/\lambda$, which however leads to the worsening of the instrumental resolution. Nevertheless, SANS provides unique advantages due the possibilities offered by the contrast variation, especially between the hydrogen isotopes. Therefore, SANS is an experimental method specifically used in the study of soft matter and biophysical systems, for which it delivers unique structural and morphological information. Most of the SANS diffractometers worldwide[21] work on the pinhole principle (**Figure 2A**), which enables the aimed low-Q resolution. Practically, all high-flux SANS diffractometers have a similar maximum flux on the order of 1×10^8 n cm^{-2} sec^{-1}. Based on the relaxed wavelength resolution, the KWS-2 has a nearly doubled flux[2, 4]. Recently, very specialized SANS diffractometers became operational to serve with optimized characteristics for a specific range of applications, such as for investigations at very small scattering vectors[22, 23]. With the very recent commission of the specialized TOF-SANS diffractometers at steady-state reactors[24] or spallation sources [25, 26], a massively-increased dynamic Q range in a given experimental setup and increased flexibility and optimization regarding the choice of the experimental resolution are offered. For the KWS-2 SANS diffractometer, a high level of versatility and performance required for very specific structural studies in the field of soft matter and biophysics is enabled on an otherwise classical SANS instrument. The optimization, flexibility, and spontaneity in designing and conducting complex studies, as supported by the described protocol, is achieved through the combination of the optimized experimental parameters *(e.g.,* intensity, length scale, space resolution, and time resolution) and the complex sample environments. Using the multiple working modes enumerated in the Introduction and supported by the results presented in **Figures 8-15**, the KWS-2 enhances in an easy and practical manner the performance of a classical SANS diffractometer at a steady neutron source (reactor) beyond the conventional limits of such instruments.

This protocol presents the steps that a regular user must carry out to define and conduct a simple experimental program that involves only the investigation of samples at ambient thermodynamic conditions (temperature, pressure, relative humidity) and under static conditions (no kinetics of structure formation or transformation, no shear or flow). Several temperature-controlled holders or special sample environments (**Table 1** and **Supplementary Figure 19**), such as pressure cells, rheometers, or humidity cells, are available and can be optimally installed and adjusted with special assistance from the instrument team. This protocol does not provide instructions about the settings and controls of such equipment. The definition and activation of external controllers require the use of another, more complex protocol. This protocol presents the case of working with quartz sample cells of a narrow rectangular shape (**Figure 3**). However, a broad range of cell geometries and types (**Supplementary Figure 19**) is offered to users, in order to provide increased flexibility and efficiency in conducting the experiments. In the case of using such cells, the present protocol may be followed with the adjustment of the parameters discussed in step 4.2.2. The measurement control software has been developed to offer the users increased flexibility in pursuing their scientific goals and optimization in the technical operation of the instrument. All adjustments and configurations of special functions and components of the instrument are done by the instrument team. The involvement of the scientific users in the configuration, definition, and utilization of the instrument is simplified and specifically limited only to those aspects that are in connection with the scientific issues of the experimental session. Configuration files are predefined in order to cover all special experimental issues, such as the positioning of special holders in the beam, the sample positioning in the beam (coordinates x, y,

Φ, and ω on the sample stage, rotation table, or cradle in **Supplementary Figure 5**), the adjustment of the detector and beam-stop positions for different wavelengths, the adjustment of the chopper parameters (frequency and opening window) for different wavelengths, the detection distances and aimed resolution, *etc*. Also, the current protocol does not describe how the real-time mode can be used on the KWS-2. The use of a more complex protocol is also required in order to conduct time-resolved SANS experiments.

Furthermore, this protocol presents how the measured data can be corrected for different scattering contributions from the instrument and the references and calibrated in order to obtain the sample's differential scattering cross section, $d\Sigma/d\Omega$, expressed in cm^{-1}. This quantity contains the entire structural and morphological information about the sample and is measured over a wide Q range corresponding to a broad length scale, over which structural correlations and interrelated size-levels characteristic of the investigated system appear. The scattering cross section $d\Sigma/d\Omega$ thus relates the intensity measured in a static scattering experiment at an angle Θ, $I_s=f(\Theta)$ to the structural properties of the sample.

For the evaluation of $d\Sigma/d\Omega$ for a system of interest, besides the measurement of the system, additional measurements are needed in order to correct the data for any external scattering (*i.e.*, environment, sample cell, solvent or buffer solution in the case of solute systems, *etc.*) and to calibrate the corrected data in absolute units[8]. The external background (sample cell or container), the reference sample (solvent or buffer solutions), the sample transmission (needed for the correct background subtraction and calibration of the corrected results in absolute units), the electronic background of the detector, the detector sensitivity (inhomogeneity in detector efficiency that is inherent for area detectors), and the normalized standard sample should also be measured. For the KWS-2, Plexiglas (PMMA) is used as standard sample. This is the so-called secondary standard and is periodically calibrated against a primary standard sample, which is vanadium. Vanadium delivers a very weak scattered intensity and requires very long measurement times for collecting the appropriate statistics; therefore, it is impractical for SANS purposes. The intensity collected from the sample of interest I_S and from the standard sample I_{St} can be expressed as follows:

$$I_S(counts, \theta, Q) = I_0 t_S A_S T_S \Delta \Psi_S (d\Sigma/d\Omega)_S \quad [1]$$

$$I_{St}(counts, \theta, Q) = I_0 t_{St} A_{St} T_{St} \Delta \Psi_{St} (d\Sigma/d\Omega)_{St} \quad [2]$$

where I_0 represents the incoming intensity (delivered by the collimation system), t is the thickness, A is the area exposed to the beam, T is the transmission, and $\Delta\psi$ is the solid angle at which a detection cell is seen from the sample position. If both sample and standard are measured in the same conditions with respect to the incoming beam (*i.e.*, L_C, A_C and A_S, and λ and $\Delta\lambda/\lambda$), I_0 and A are the same and the solid angle is expressed as A_D/L_D (with A_D representing the area of a detection cell). By dividing the two relations, the scattering cross-section of the sample is obtained as:

$$(d\Sigma/d\Omega)_S = \frac{t_{St}T_{St}(d\Sigma/d\Omega)_{St}}{t_S T_S} \frac{(L_D^S)^2}{(L_D^{St})^2} \frac{((I_{S+Cell}-I_B)-T_S(I_{ECell}-I_B))}{\langle I_{St}\rangle} = k \frac{((I_{S+Cell}-I_B)-T_S(I_{ECell}-I_B))}{T_S\langle I_{St}\rangle} \quad [3]$$

where the I_{St} is expressed as an average (the standard as an incoherent scattering system delivers a flat scattering pattern). The I_S is obtained after correcting the measured intensity of the sample in the cell (container) with respect to the contribution of the empty cell I_{ECell} and the background on the detector for the closed beam, I_B. The factor $t_{St}T_{St}(d\Sigma/d\Omega)_{St}$, which contains the scattering and physical parameters of the standard sample, depends on the neutron wavelength λ and is typically known from the calibration of the standard sample. Thus, it is tabulated in the data reduction software[4]. The parameters and quantities in Eq. 3 that are known from calibration procedures and the definition of the experimental setup (t_S, L_D) form the so-called calibration factor k. The intensities and the sample transmission T_S that appear in Eq. 3 must be measured. The data analysis program qtiKWS enables the correction, calibration, and radial averaging of the experimental data and the achievement of $d\Sigma/d\Omega$ for the investigated samples in a flexible and versatile working mode. The final results generated with the qtiKWS software are presented as tables with four columns: Q, I, ΔI, $\Delta\sigma$ where I represents $d\Sigma/d\Omega$ and $\Delta\sigma$ is the Q resolution[5].

From a practical point of view, with the KWS-2, combined SANS and USANS investigations can be carried out, with the advantage that the sample geometry and the thermodynamic conditions remain constant. Large morphologies that show multiple structural levels spanning a wide length-scale from nanometer to micrometer sizes can be investigated in a direct way, as shown in **Figure 12**. Besides the small-scale structural limit R_C observed in the scattering curve measured in the conventional pinhole mode, by activating the lenses and the high-resolution detector, the large-scale structural limit L_C of cylindrical core-shell micelles formed by the poly-(hexylene-oxide-co-ethylene-oxide) PHO10k-PEO10k diblock copolymer (fully protonated) in D_2O[14] could be observed at very low Q values in the extended Q-range working mode. The cylindrical micelles are characterized by a total thickness of about 300 Å and a length of about 7,000 Å, as revealed by the fit of the experimental results with the core-shell cylindrical form-factor[9,14]. Therefore, certain sensitive effects such as thermo-responsive gels or formation and growth of crystalline or partially-crystalline morphologies can be unambiguously explored with the KWS-2, unlike the classical approach of involving two or more different instruments and sample geometries.

As presented in **Figure 11**, correlated systems and ordered structures can be studied with adapted resolutions in a very flexible way, without spending time and effort on the installation of complex monochromatization systems, which would involve additional care and safety aspects. Moreover, by involving the chopper and the TOF data acquisition mode, monodisperse soft matter systems or complexes with low size polydispersity can be characterized very precisely at still-high intensities[5].

The hindrances generated by the weak scattering due to use of highly-diluted systems or unfavorable contrast conditions can be overcome by the use of even higher intensities based on the larger beam size on the sample, while keeping the resolution. **Figure 13A** reports the scattering patterns from polystyrene particles of a radius of R = 150 Å, measured in the high-intensity mode using the lenses and a quadratic beam size ranging between 10 mm x 10 mm, the typical size used in the conventional pinhole mode, and 30 mm x 30 mm. Additionally, the result from a measurement with a round beam 50 mm in diameter (full lens size) is shown. In parallel, the normalized result obtained in the conventional pinhole mode is presented. Using 26 lenses with neutrons of λ= 7 Å and the same entrance aperture size A_C as for the conventional pinhole mode (**Figure 2B**), a gain in intensity on the sample of about 12 times is obtained while keeping a constant beam size (resolution) on the detector, as shown in **Figure 13B-C**. The 27-lens system has a transmission of about 32% at ambient temperature. Cooled down to a temperature of 50 K, the lens transmission increases due the suppression of scattering on phonons in the lens material. The system of 26 parabolic lenses has a transmission of about 65% for a round beam size of 50 mm, when the beam goes through the entire volume of the lens,

and of about 92% for a quadratic beam size of 10 mm x 10 mm, when only a very amount of lens material stays in the beam. The high-intensity mode with lenses offers benefits in the case of weak scattering that generally is encountered at a large detection distance and is particularly problematic in the case of weak contrast conditions. Additionally, when the sample is only stable over short period of times, the use of this mode represents a clear advantage, as is demonstrated elsewhere[15].

On the other hand, in the case of biological systems, small sample volumes are typically available for experiments. Small biological molecules in physiological conditions with sizes of a few nanometers deliver weak scattering signals above the dominant scattering from the buffer solutions. Such signals can be measured with the KWS-2, benefiting from the high intensity of the instrument in the low-resolution setup of the pinhole mode, using short collimation lengths L_C = 2 m or 4 m and short detection distances L_D = 1 m, 2 m, or 4 m. **Figure 14** presents the scattering patterns from beta amyloid protein (Aβ 1-42, M_W = 4.5 kDa) monomers in deuterated hexafluoroisopropanol dHFIP, as obtained after the correction for the scattering signal from the buffer was applied. A model fit of the data delivered a monomer size of about 16 ± 1 Å[16]. A long measurement time of several hours for each experimental condition (detection distance L_D and sample type) was involved, although the measurements were carried out at short detection distances. The old detector, which has shown limitations regarding the count rate, hindered the use of short collimation distances L_C, hence the use of the maximum flux at the instrument. With the commission of the new detection system enabling the use of the full neutron flux, such weak intensities will be measured in shorter times and with improved statistics in the future.

Finally, stimuli-sensitive effects can be studied in a flexible and easy manner by using the special ancillary equipment of the KWS-2. An example is reported in **Figure 15**, which shows the SANS patterns from Lysozyme protein in D_2O buffer and from the buffer collected at different pressures. Special attention has been paid to the investigation of the background and forward scattering from the Lysozyme molecules, used in the performance test of the new pressure cell manufactured in-house by following a design done by PSI, Switzerland. The results were similar to those obtained by Kohlbrecher *et al.* in a similar study to test the original pressure cell model constructed there[17, 18]. With the KWS-2, further data has been acquired since a pressure of 5,000 bar has been reached. Evolution of the forward scattered intensity from the protein follows a linear behavior, as observed in the study at PSI, Switzerland[18].

Disclosures

The authors have nothing to disclose.

Acknowledgements

References

1. Gläser, W., & Petry, W. The new neutron source FRM II. *Physica.* B **276-278**, 30-32 (2000).
2. Radulescu, A., Pipich, V., & Ioffe, A. Quality assessment of neutron delivery system for small-angle neutron scattering diffractometers of the Jülich Centre for Neutron Science at FRM II. *Nucl. Instrum. Methods Phys. Res. Sect.* A **689**, 1-6 (2012).
3. Radulescu, A., & Ioffe, A. Neutron guide system for small-angle neutron scattering instruments of the Jülich Centre for Neutron Science at FRM-II. *Nucl. Instrum. Methods Phys. Res. Sect.* A **586**, 55-58 (2008).
4. Radulescu, A., Pipich, V., Frielinghaus, H., & Appavou, M. S. KWS-2, the high intensity/wide Q-range small angle neutron diffractometer for soft-matter and biology at FRM II. *J. Phys.: Conf. Ser.* **351**, 012026 (2012).
5. Radulescu, A., et al. Tuning the instrument resolution using chopper and time of flight at the small-angle neutron scattering diffractometer KWS-2. *J.Appl.Cryst.* **48**, 1849-1859 (2015).
6. Frielinghaus, H., et al. Aspherical refractive lenses for small-angle neutron scattering. *J. Appl. Cryst.* **42**, 681-690 (2009).
7. Radulescu, A., Fetters, L.J., & Richter, D. Structural characterization of semicrystalline polymer morphologies by imaging-SANS. *J.Phys.: Conf.Ser.* **340**, 012089 (2012).
8. Zemb, T., & Lindner, P. *Neutron, X-rays and Light Scattering Methods Applied to Soft Condensed Matter.* Elsevier Science. 552 (2002).
9. Pedersen, J. S. Analysis of small-angle scattering data from colloids and polymer solutions: modeling and least square fittings. *Adv. Colloid Interface Sci.* **70**, 171-210 (1997).
10. Barker, J. G., & Pedersen, J. S. Instrumental Smearing Effects in Radially Symmetric Small-Angle Neutron Scattering by Numerical and Analytical Methods. *J. Appl. Cryst.* **28**, 105-114 (1995).
11. Hammouda, B., & Mildner, D. F. R. Small-angle neutron scattering resolution with refractive optics. *J. Appl. Cryst.* **40**, 250-259 (2007).
12. Vad, T., Sager, W. F. C., Zhang, J., Buitenhuis, J., & Radulescu, A. Experimental determination of resolution function parameters from small-angle neutron scattering data of a colloidal SiO_2 dispersion. *J. Appl. Cryst.* **43**, 686-692 (2010).
13. Amann, M., Willner, L., Stellbrink, J., Radulescu, A., Richter, D. Studying the concentration dependence of the aggregation number of a micellar model system by SANS. *Soft Matter.* **11**, 4208-4217 (2015).
14. Ströbl, M., *Diploma Thesis.* Univ. Regensburg, Germany (2008).
15. Dahdal, Y. N., et al. Small-Angle Neutron Scattering Studies of Mineralization on BSA Coated Citrate Capped Gold Nanoparticles Used as a Model Surface for Membrane Scaling in RO Wastewater Desalination. *Langmuir.*, **30**, 15072-15082 (2014).
16. Zhang-Haagen, B., et al. Monomeric Amyloid Beta Peptide in Hexafluoroisopropanol Detected by Small Angle Neutron Scattering. *PLOS One.* **11**, e0150267 (2016).
17. Kaneko, F., Radulescu, A., & Ute, K. Time-resolved small-angle neutron scattering on guest-exchange processes in co-crystals of syndiotactic polystyrene. *J. Appl. Cryst.* **47**, 6-13 (2014).

18. Kohlbrecher, J., et al. A high pressure cell for small angle neutron scattering up to 5000 MPa in combination with light scattering to investigate liquid samples. *Rev. Sci. Instr.* **78**, 125101 (2007).

19. Vavrin, R., et al. Structure and phase diagram of an adhesive colloidal dispersion under high pressure: A small angle neutron scattering, diffuse wave spectroscopy, and light scattering. *J. Chem. Phys.* **130**, 154903 (2009).

20. Kaneko, F., et al. Development of a Simultaneous SANS/FTIR Measuring System. *Chem. Lett.* **44**, 497-499 (2015).

21. *SAS Portal.* www.smallangle.org (2016).

22. Goerigk, G., & Varga, Z. Comprehensive upgrade of the high-resolution small angle neutron scattering instrument KWS-3 at FRM II. *J. Appl. Cryst.* **44**, 337-342 (2011).

23. Desert, S., Thevenot, V., Oberdisse, J., & Brulet, A. The new very-small-angle neutron scattering spectrometer at Laboratoire Léon Brillouin. *J. Appl. Cryst.* **40**, s471-s473 (2007).

24. Dewhurst, C. W. D33 - a third small-angle neutron scattering instrument at the Institute Laue Langevin. *Meas. Sci. Technol.* **19**, 034007 (2008).

25. Zhao, J. K., Gao, K. Y., & Liu, D. The extended Q-range small-angle neutron scattering diffractometer at the SNS. *J. Appl. Cryst.* **43**, 1068-1077 (2010).

26. Takata, S., Suzuki, J., Shinohara, T., Oku, T., Tominaga, T., Ohishi, K., Iwase, H., Nakatani, T., Inamura, Y., Ito, T., Suzuya, K., Aizawa, K., Arai, M., Otomo, T., & Sugiyama, M. The Design and q Resolution of the Small and Wide Angle Neutron Scattering Instrument (TAIKAN) in J-PARC. *JPS Conf. Proc.* **8**, 036020 (2015).